Carbohydrate Polymers 328 (2024) 121743

Contents lists available at ScienceDirect

Carbohydrate Polymers

journal homepage: www.elsevier.com/locate/carbpol

Starch-fibers composites, a study of all-polysaccharide foams from microwave foaming to biodegradation

Ana Isabel Quilez-Molina [a,b,*], Jean François Le Meins [a], Bertrand Charrier [c], Michel Dumon [a,**]

[a] Laboratoire de Chimie des Polymères Organiques, University of Bordeaux, CNRS, Bordeaux INP, LCPO UMR 5629, F-33607 Pessac, France
[b] BioEcoUVA Research Institute on Bioeconomy, University of Valladolid, Spain
[c] University of Pau and the Adour Region, E2S UPPA, CNRS, Institute of Analytical Sciences and Physico-Chemistry for the Environment and Materials-Xylomat, IPREM-UMR5254, 40004 Mont de Marsan, France

ARTICLE INFO

Keywords:
Flax
Cellulose
Pulping
Microwave
Long fibers
Starch composites
Bio-based foams

ABSTRACT

Sustainable composite foams based on rice starch and cellulosic long fibers were successfully fabricated using microwave irradiation. They were presented as a promising method to recycle some of the textile industry waste. A deep study of the processability and functionality of the composites revealed the performance improvement of starch with the addition of long cellulosic fibers, especially with 6 wt% of Arbocel®, in terms of foamability, water, and mechanical resistance features. Moreover, sodium bicarbonate, which acted as a blowing and pulping agent, led to a lower density and better fiber distribution that resulted in an improvement of the foams' functionalities. The range of the study is new in the domain of long fiber foam composites in terms of the foaming capability, and mechanical, thermal, and water resistance properties. Furthermore, all foams showed excellent biodegradability properties against a fungus commonly found in the environment; for example, values around 60 % weight loss after 33 days. Finally, the assessment of the CO_2 emission during the process underlines the environmental benefits of the method employed.

1. Introduction

In "dynamic" foamable systems, the cumulation of several properties (lower weight, water sensitivity, mechanical strength, biodegradability) is indeed a difficulty. Many factors and mechanisms compete and interact in opposite or synergetic ways: initial viscosity; fiber type, content, and length; as well as interactions between components of the formulation, in particular, via a competitive behaviour of H-bonding between the numerous hydroxyl bonds (cellulose, water, starch).

On the other hand, all polysaccharide foam composites filled with long continuous or discontinuous cellulose fibers represent a sustainable way to carry out the recycling of textile fibers. Indeed, the textile industry is considered the fifth largest contributor to carbon emissions, producing 10 % of the total carbon emissions (Juanga-Labayen, Labayen, & Yuan, 2022). Regarding waste management, 75–85 % of the textile waste is disposed of in landfills, 25–15 % is reused or recycled, and <1 % is recycled back into clothing (Espinoza Pérez, Espinoza Pérez, & Vásquez, 2022; Mu & Yang, 2022; Négrier, El Ahmar, Sescousse, Sauceau, & Budtova, 2023; Völtz, Berglund, & Oksman, 2023). The residues of textile fibers can be advantageously used as composite reinforcements providing better mechanical properties to the composite (Bergel, Araujo, & Santana, 2021; van Rijswijk & Bersee, 2007). However, the reprocessing of fibers as fillers is often limited by either the lack of impregnation with the matrix, low dispersibility, or lower thermal resistance for being processable with many polymers (Bergel et al., 2021; van Rijswijk & Bersee, 2007). A great challenge of reprocessing fiber tissues has been associated with the heterogeneous chemical composition present in textile fibers, which arrangement, content, and concentration in different carbohydrates (i.e., cellulose, lignin, hemicellulose, pectin) change with the type of tissue (Alam & Christopher, 2017; Foulk, Chao, Akin, Dodd, & Layton, 2006). For example, cotton-like fibers are mainly composed of cellulose fibers (about 95 wt%), while flax fibers are a self-contained composite that consists of a bundle of cellulose fibers reinforced with non-cellulosic components, i.e. pectin (Foulk et al., 2006; Zimniewska, Rozańska, Gryszczynska, Romanowska, & Kicinska-Jakubowska, 2018). This results in different recycling pre-

* Correspondence to: A. I. Quilez-Molina, BioEcoUVA Research Institute on Bioeconomy, University of Valladolid, Spain.
** Corresponding author.
E-mail addresses: anaquilezm@gmail.com, anaisabel.quilez@uva.es (A.I. Quilez-Molina), lemeins@enscbp.fr (J.F. Le Meins), bertrand.charrier@univ-pau.fr (B. Charrier), michel.dumon@u-bordeaux.fr (M. Dumon).

https://doi.org/10.1016/j.carbpol.2023.121743
Received 9 November 2023; Received in revised form 24 December 2023; Accepted 26 December 2023
Available online 29 December 2023

Table 1
The labelling and characteristics of the long cellulosic fibers. The data is provided by the suppliers.

Cellulose fiber Reinforcement	Average Length (L)	Average Diameter (D)	Estimated average aspect ratio (L/D)	Content of cellulose (%)	Apparent bulk density (g/cm^3)
A-F400	2000 μm	35 μm	57	99.5	0.025–0.05
F	3.4 cm = mould dimension	20 μm is the average unitary filament diameter	~ 1700	70–80	1.5

treatments that include some highly toxic and hazardous chemicals, such as carbon disulfide (CS_2) or ammonium (Alam & Christopher, 2017). Alkaline treatment is the most popular and cost-effective method to obtain high-performance natural fibers and it is included in the recyclizing procedure of textile and paper fibers (Adu, Jolly, & Thakur, 2018; Chen et al., 2017). The basic pulping removes the hemicellulose and lignin, incrementing the availability of hydroxyl groups present in cellulose to interact with a hydrophilic polymeric matrix (Chen et al., 2017).

The employment of sodium bicarbonate ($NaHCO_3$) as a basic pulping agent of cellulosic fibers, before loading into a polymer matrix, is a sustainable strategy to pretreat the cellulosic fibers. In addition to this, $NaHCO_3$ has been also widely employed to obtain low-density porous polymeric composites, acting as a blowing agent by thermally degrading into CO_2, H_2O, and Na_2CO_3 (Bergel et al., 2021; Saed Hussein et al., 2019; Wei et al., 2023). The foaming properties of $NaHCO_3$ were observed by (Saed Hussein et al., 2019), where this chemical reduced the density of an epoxy resin obtained up to 3 times. This blowing agent has been employed to improve the properties of sustainable polymeric materials, such as the bactericide properties of Materbi®-carvacrol composites (Lopresti et al., 2019), or the expansion capability of starch-based foams (Georges, Lacoste, & Damien, 2018; Robin et al., 2010).

The great compatibility of starch with cellulosic compounds, derived from their chemistry, based on units of glucose that form chains of amylopectin and amylose biopolymers, has been already proved in numerous articles that include starch-based foams loaded with cellulosic-based fibers (Bergel et al., 2021; Ji et al., 2021; Peng et al., 2022). These studies confirmed that fibers influence the foaming mechanism of starch, changing the size and distribution of pores, and hence, their final properties. The foaming mechanism of starch starts with the diffusion of water molecules into the amorphous region of the semicrystalline starch granules when the MW heating conditions reach the gelatinization temperature (around 70 °C). This results in starch gelatinization (i.e., disruption of the molecular order of the starch granules), which includes the cleavage of intermolecular bonds, structural rearrangements, and the formation of new interactions with the solvent. Afterwards, when the temperature exceeds the boiling point of water, the inner moisture is transformed into superheated steam bubbles that expand, creating a cellular structure and a solid foam (Soykeabkaew, Thanomsilp, & Suwantong, 2015; Wani et al., 2012). Recently published articles have already employed the characteristic properties of rice starch to create materials with advanced properties, such as super absorbent foams (Q. Zhang et al., 2020), batteries (Escamilla-Pérez et al., 2023), and which highlighted good performance properties in combination with cellulosic fibers (Almeida et al., 2019; F. L. Chen et al., 2022). Rice starch is considered an important source of starch (about 80 %), cheaper and more available than other starches (Wani et al., 2012; Zhang et al., 2020). Moreover, rice production generates about 15–20 % of broken rice, commonly used for animal feeding, that can be used for developing new materials, preventing the employment of other edible and more demanded starches (e.g., corn, cassava) for a non-nutritional purpose (Wani et al., 2012; Zhang et al., 2020).

However, despite the high potential of starch foams to substitute petroleum-derived polymers in fields such as food packaging and drug delivery systems (Soykeabkaew et al., 2015). Few studies include a complete analysis of the effect of long cellulosic fibers (from 2 mm) on different parameters that can provide useful information for the processability and applicability of the starch foams (Peng et al., 2022). According to them, the improvement in the porosity, processability, and functional properties of starch foam composites (i.e., biodegradability and mechanical resistance) with the addition of long fibers (neat or pulped with $NaHCO_3$) is expected. Moreover, starch foaming is assisted by microwave irradiation, whose highly effective internal heating reduces the exposure time and energy becoming an eco-friendly and save-costing manufacturing technique. Moreover, the low exposure time, reduced from hours to minutes/s, is favorable for thermal-sensitive fillers (Naik, Singh, & Sharma, 2022; Yu et al., 2021). Lastly, microwave irradiation can have a positive effect on enhancing the pulping effect of alkaline reagents on fibers, as previously shown (Dong et al., 2022).

Sodium hydrogen carbonate ($NaHCO_3$) will be tested, as an edible and green chemical, to act as a pulping agent, improving the dispersion and compatibility of the fibers with the starch matrix and as a blowing agent, promoting the formation of pores and reducing the material density, obtaining cellulosic fibers-starch foams composites with excellent functional properties. The effect of $NaHCO_3$ will reveal more noticeable in flax fibers as a result of the removal of non-cellulosic components, despite that, all fibers (neat or pulped) enhanced the fibers' dispersity, the expansion ratio, and reduced the water sensitivity of starch foams. Last but not least, the study of the environmental impact of these materials was performed by quantifying the composites' biodegradability and greenhouse gas emissions.

The overall objective is to provide a complete analysis, from processing to degradation, of all polysaccharide foam composites filled with long continuous or discontinuous cellulose fibers; as new sustainable foam products using an eco-friendly and low-cost method.

2. Materials and methods

2.1. Materials

Long discontinuous cellulose fibers were kindly provided by JRS Rettenmaier (France): pure cellulose (99.5 % cellulose) Arbocel® FIF 400, labelled as A-F400, with an average length of 2000 μm and fiber diameter of 35 μm. Terre de Lin / Safilin (France) kindly provided flax yarns (labelled as F) from a textile wire spool, whose chemical composition was about 0.6–1.0 % pectin, 2.5–3.0 wt% lignin, 70–80 wt% cellulose and 14–20 wt% hemicellulose (Zimniewska et al., 2018). The yarns of F fibers were carefully separated and cut in the same length as the container that will determine the final size of the foams (i.e., 3.4 cm), to fill the whole final foamed material with one “single” fibers' network. Generally, a single flax fiber length varies from 4 mm to 80 mm, and a unitary fiber diameter of 20 μm which individual fibers are linked by pectin (Poilâne et al., 2014). Before mixing with starch and foaming, a bulk dry interweaved network of microfibers is realized. Table 1 summarizes the main characteristics of the reinforcements (A-400 and F) used in this article. A native Rice starch (labelled as RS) was provided by Sigma Aldrich. Rice starch has been chosen because it possesses a high amylopectin/amylose ratio (17–29 % of amylose) that provides suitable expansion properties and rather low density to the foams. This occurs because amylopectin has better water-holding capacity, providing good swelling properties and sufficient strength to trap bubbles and create pores (Chen, Xie, Liu, & Chen, 2019; Soykeabkaew et al., 2015; Wani

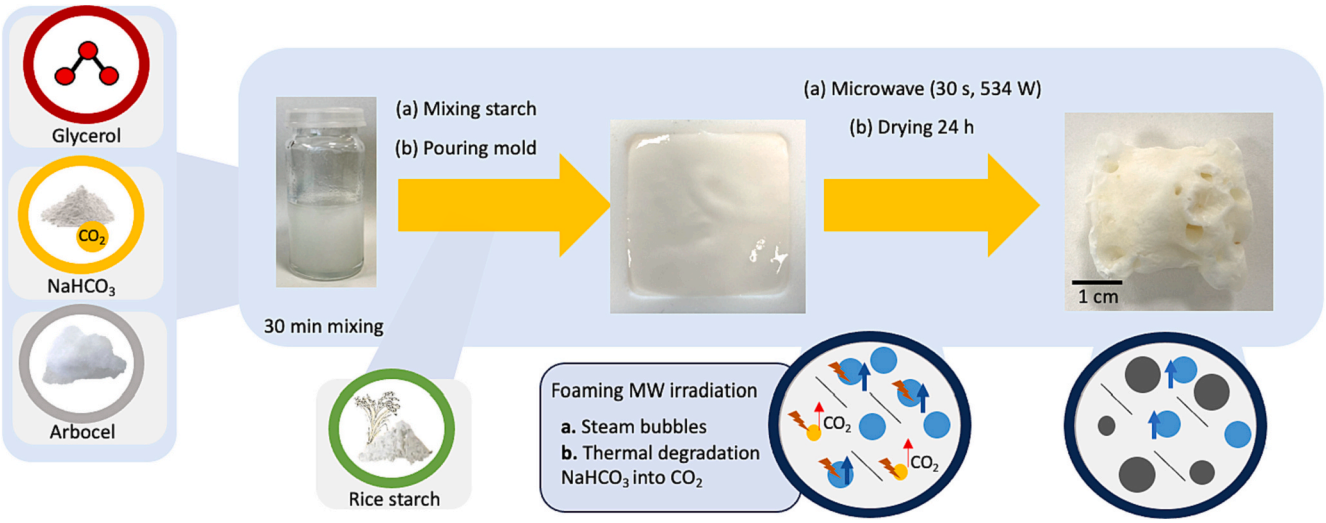

Fig. 1. The scheme of the fabrication process of starch-cellulose foams. The blue circles represented the steam bubbles, the yellow circle represented the sodium bicarbonate, the lines indicated the fibers and the orange lightning represented the microwave irradiation. (For interpretation of the references to color in this figure legend, the reader is referred to the web version of this article.)

et al., 2012). Moreover, its small granule size (about 3–8 μm) is known to provide a better mechanical performance in comparison with other starches with larger granules (Lee et al., 2009). The plasticizer glycerol was selected as a non-volatile plasticizer, increasing the durability of the polymer's mechanical characteristics (Prabhakar, Rehman Shah, & Song, 2017).

2.2. Starch-cellulose composites foamed through microwave (MW) irradiation

The composite foams were obtained employing two different free-expansion fabrication methods adapted from (Tacha et al., 2023).

2.2.1. Water as the only blowing agent

For the preparation of the materials, 2.8 g of the plasticizer glycerol was put to stir at 300 rpm in a hot plate (Hei-PLATE Mix 20) with 9.6 g of water (giving a solution at 22.6 wt% of glycerol), for 5 min until obtaining a clear solution. Then, A-F400 was added in two different concentrations, 2 and 6 wt% with respect to the starch, which was added in the last step. F fibers were prepared only in 2 wt% because the 6 wt% overcame the mould volume capacity, see Fig. S1 of Supporting information. All these ingredients were mixed for 30 min at 700 rpm on the hot plate (Hei-PLATE Mix 20). Then, they were mixed in a manual mode with 11.4 g of RS to obtain a homogeneous and viscous starch batter, in which the concentration of starch in the mixing solution is 47.9 wt%. This starch batter was subsequently poured into a mould of polytetrafluoroethylene (PTFE) ($3.4 \times 3.4 \times 1.4$ cm^3) until the complete filling ($\sim$ 12 g). The PTFE mould was placed in a standard microwave (AYA MO-22 AL) for 30 s, at 534 W. The MW conditions (i.e., powers and time) were optimized to obtain the best foam expansion, avoiding the excessive heating that could result in the burn of the sample, see the photograph of the sample treated at 700 W for 45 s in Fig. S2 of Supporting information). Finally, the product was carefully removed from the mould and the starch composite foam obtained was left to dry under the hood at room temperature for 24 h to allow the evaporation of most of the remaining water molecules, $\sim$ 30 wt% for all samples, independently to the fiber type and concentration. The same values of water loss were observed in other starch foams enriched with cellulosic fibers (Lopez-Gil, Silva-Bellucci, Velasco, Ardanuy, & Rodriguez-Perez, 2015). Starch foams were kept in polyethylene (PE) zip bags until their characterization.

2.2.2. Water and sodium bicarbonate as blowing agents

The scheme of Fig. 1 displays the production process of starch-composite foams using A-F400 filler as an example. Following the fabrication steps explained above, 2.8 g of glycerol and 0.57 g of hydrogen sodium carbonate or sodium bicarbonate $NaHCO_3$ (in water, the hydrogen carbonate ion HCO_3^-), plasticizer, and foaming agent respectively, were put to stir at 300 rpm in 9.6 g of water for 5 min until obtaining a clear solution. Note that the global concentration in weight is not the same (21.6 wt%) because of the presence of $NaHCO_3$. The basic character of the foaming agent sodium bicarbonate raised the pH to 8.5. Then, different quantities of the commercial cellulose fibers (2 and 6 wt% regarding the starch fraction) were mixed with the previous solution for 30 min at 700 rpm (Hei-PLATE Mix 20). After manually mixing with 11.4 g of RS, the homogeneous batter was placed in a mould of polytetrafluoroethylene (PTFE) ($3.4 \times 3.4 \times 1.4$ cm^3), and placed in a microwave (30 s, 534 W). As shown in the scheme of Fig. 1, the starch-cellulose mixture filled the mould cavity, however, as a consequence of the expansion effect of the microwave irradiation, part of the foam flashed out of the mould. However, this effect was not undesirable because it facilitated the interpretation of the expansion capability of each sample. In the presence of $NaHCO_3$, the foaming involved two mechanisms: the formation and growth of steam bubbles, observed also in the fabrication method explained above, and the thermal decomposition of $NaHCO_3$, which thermal degradation results in the release of CO_2 gas (Tacha et al., 2023). Samples are labelled RS_xfiber-name_CO_3 which stands for RS: rice starch, x: mass percentage of fibers, F400: cellulose Arbocel® A-F400, F: flax, CO_3: addition of $NaHCO_3$.

2.3. Foam starch composites characterization

2.3.1. Amylose content

The amylose content of rice starch used was measured at INRAE Nantes (Biopolymères Interactions Assemblages), Matériaux, Création & Comportement (MC2) by a calorimetric method, i.e. the enthalpy measurement of an amylose/lipid (LPC) complex. Amylose has a water content of 11 % determined by thermobalance before DSC analysis. An 8 % L-α-lysophosphatidylcholine (LPC) solution was prepared. Its enthalpy was calculated using the DSC Q200 apparatus (TA-waters instruments) using the method reported by (Mestres, Matencio, Pons, Yajid, & Fliedel, 1996) with slight modifications: A 60 μL pan of starch water/LPC solution, against a 60 μL reference pan of pure water, was scanned by DSC. The temperature was increased up to 140 °C at a rate of

10 °C/min, followed by an isotherm of 2 min, and temperature was decreased to 20 °C at a rate of 3 °C/min. This cycle was repeated two times. Upon heating, all amylose melts; upon cooling, all amylose crystallizes in the form of an amylose/LPC complex, which is then measured. Enthalpy obtained was calculated using the software TA Instrument Universal Analysis, obtaining ΔH = 6.809 J/g at 89.26 °C, which corresponded to 25.5 % of amylose (average of two samples). The DSC curves are reported in Fig. S3 of Supporting information.

2.3.2. Apparent density and expansion ratio

The apparent density of the foams was calculated by dividing the masses by the volumes of the foams, in triplicate for each sample. The density was calculated after 24 h to allow the foam structure to dry and set when most of the water molecules (in around 30 % of the total foam weight) were evaporated and following Eq. (1):

$$\text{Foam density}\left(\frac{g}{cm^3}\right) = \frac{W_f}{V_f} \quad (1)$$

where w_f is the foam mass (g) and v_f is the foam volume (cm^3).

The expansion ratio was calculated following Eq. (2), as reported elsewhere (Gimeno, Moraru, & Kokini, 2004):

$$\text{Expansion ratio} = \frac{V_f}{V_1} \quad (2)$$

where V_f is the volume of the pre-foamed batter and V_f is the volume of the foam after 24 h of drying.

2.3.3. Viscosity of initial formulation before foaming

The rheological behaviour of the starch batter was measured using a stress-controlled rotational rheometer (Anton Parr MCR302) plate geometry (∅=25 mm) was chosen with a gap around 1 mm, regarding the characteristic size of the cellulose fiber used at 20 °C. In a first attempt shear rate sweeps were performed from 0,01 s^{-1} to 100 s^{-1} to characterize the viscosity versus shear rate in a relatively large range of shear flow. This protocol revealed complex behaviour that was not easily repeatable, probably because of stationary state issues or thixotropy. Therefore, a constant shear rate during 2 min at different values (0.1; 0.5; 1.0, and 5.0 s^{-1}) was applied in order to check whether the viscosity was measured in a steady state or not. Each measurement was performed in triplicate.

2.3.4. Scanning electron microscopy (SEM)

The morphological study of the samples was performed using a scanning electron microscope (SEM) was employed (model HITACHI S-3000 N). For the preparation of the samples, foams were frozen in liquid nitrogen and fractured to ensure that the microstructure remained intact. Surfaces were coated with gold using a sputter coater (model EMSCOPE SC 500), in an argon atmosphere. The average cell size and cell density (number of cells per volume unit) of the analyzed foams were calculated using the ImageJ software. Cell density was calculated using Eq. (3) following the method published elsewhere (Pinto, Dumon, Pedros, Reglero, & Rodriguez-Perez, 2014):

$$N_f = \left(\frac{nM^2}{A}\right)^{3/2} \cdot \frac{1}{1 - V_f} \quad (3)$$

Being V_f calculated using Eq. (4):

$$V_f = 1 - \frac{\rho_f}{\rho_p} \quad (4)$$

where Nf is the cell density (cells/cm^3), n is the number of cells in the micrograph, M is the magnification of the image, A is the area of the micrograph (cm^2). V_f is the void fraction/porosity, ρ_f is the density of the foam (g/cm^3), and ρ_p is the density of the non-foamed starch (g/cm^3), which corresponds to 1.50 g/cm^3 (Yildirim, Shaler, Gardner, Rice, & Bousfield, 2014).

2.3.5. Attenuated total reflection Fourier transform infrared (ATR-FTIR) spectroscopy

Infrared spectra of the fibers and pulped fibers were obtained using an Attenuated Total Reflectance (ATR) accessory (GladiATR, PIKE Technologies) coupled to a Fourier Transform Infrared (FTIR) spectrometer (Vertex 70, Bruker).

2.3.6. Thermal properties

The thermal gravimetric (TG) curves and the first derivative of the TGA curve (DTG) curve were acquired using a TA Q500 instrument. The samples (~ 20 mg) were heated from 30 to 850 °C under an inert N_2 atmosphere with a flow rate of 60 mL/min and a heating rate of 10 °C/min.

2.3.7. Moisture content, absorption isotherms at controlled RH (%), Liquid water absorption capability and water-soluble fraction

The moisture content was measured by introducing the samples with a weight (W_1) in a vacuum oven at 40 °C until reaching constant weight (W_2) as reported in our previous work (Quilez-Molina, Oliveira-Salmazo, Amezúa-Arranz, López-Gil, & Rodríguez-Pérez, 2023). The moisture content was calculated following Eq. (5):

$$\text{Moisture}\ (\%) = \frac{W_1 - W_2}{W_1}\ \text{x}\ 100 \quad (5)$$

Absorption isotherms were determined through a static gravimetric method by setting different relative humidity (RH) conditions: 43 %, 59 %, and 100 %. The controlled relative humidity was obtained by placing the samples (1.5 cm × 1.5 cm) in sealed jars with small glasses containing potassium carbonate (43 %), sodium nitrate (59 %), and water (100 %). Before each measurement, the sample was dried by conditioning at 0 % with silica gel for 96 h to ensure complete drying. Then, they were weighted after 24 h (Quilez-Molina et al., 2020). The moisture adsorption at each RH condition was calculated following Eq. (6).

$$\text{Moisture adsorption at RH}\ (\%) = \frac{W - W_0}{W_0}\ \text{x}\ 100 \quad (6)$$

where W is the weight after 24 h at each relative humidity and W_0 is the weight at 0 % RH. These measurements were performed in triplicate.

For measuring the liquid water absorption, each sample (1.5 cm × 1.5 cm) was weighed after drying in the vacuum oven for 6 h at 40 °C. Then, the foam was placed in 20 mL of distilled water for 10, 20, 45 min, and 24 h. For each time point, the sample was weighed again after removing the excess of water using tissue paper. The results of water adsorption capacity were represented in terms of g liquid water adsorbed/100 g sample at room conditions following Eq. (7):

$$\text{Liquid water absorption capability}\ (g/100g\ \text{of sample}) = \frac{W_t - W_0}{W_t}\ \text{x}\ 100 \quad (7)$$

where W_t is the weight at time t and W_0 is the weight at 0 % RH. These measurements were performed in triplicate.

Another characteristic is the water-soluble fraction, evaluated following the procedure reported in our previous work (Quilez-Molina, Mazzon, Athanassiou, & Perotto, 2022) with slight modifications. The calculation is as follows: the samples were cut in cubes (1.5 cm^2 × 1.5 cm^2), dried in a vacuum oven at 40 °C for 6 h, and weight (W_0). Then, they were immersed in 20 mL of distilled water for 24 h, dried again in a vacuum oven for 6 h at 40 °C, and weighed (W) to measure the water-soluble fraction. See Eq. (8).

$$\text{Water soluble fraction}\ (\%) = \frac{W_0 - W}{W_0}\ \text{x}\ 100 \quad (8)$$

where W is the dried weight after the immersion for 24 h, and W_0 is the

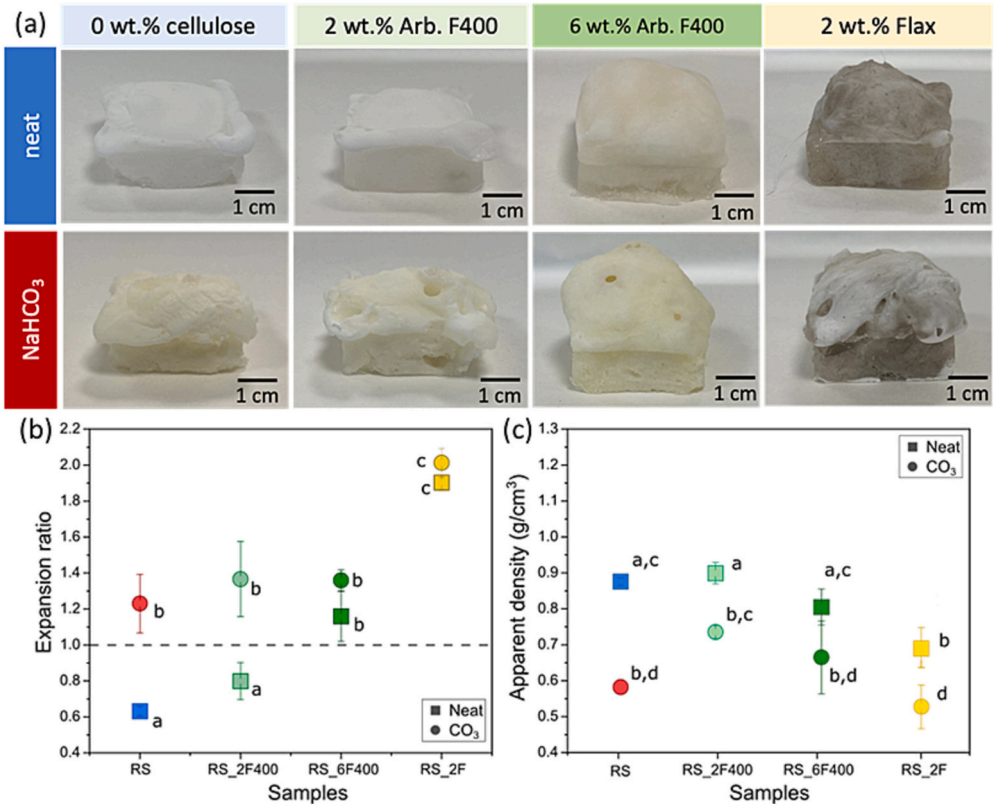

Fig. 2. (a) The photographs of the samples fabricated in this work. (b) The expansion ratio of the foamed samples, (c) The apparent density of water-foamed samples (squares) and water+$NaHCO_3$-foamed samples (circles). The same letters indicate nonsignificant differences among the results according to Tukey's test ($p < 0.05$).

weight of the dried sample. These measurements were performed in triplicate.

2.3.8. Compression test

Samples were conditioned at 20 °C and 60 % relative humidity (RH) for 48 h before the compression test. The deformation rate employed was 2.5 mm/min to a deformation of 70 % of the sample weight. The compressive strength was calculated as the maximum load divided by the cross-sectional area of the sample (Duan et al., 2022). The tested dimension is 3.4 × 3.4 cm^2. The shape recovery (%) was calculated by dividing the recovery height by the height of the sample before the compression test, as reported elsewhere (Kim, Kim, Lee, Yeom, & Lee, 2021).

2.3.9. Biodegradability test

Tablets of starch and fibers (∅=13 mm) were prepared using a Manual Hydraulic Press (Specac) by pressing up to 10 tons. Before testing, a piece of the samples (~ 1 cm × 1 cm) and the tablets were dried for 24 h at 105 °C in an oven Memmert UF55 plus-Universal. Fungal resistance was tested according to the adaptation of European standard EN 350–1 and following the procedure published elsewhere (Can, Tomak, Ermeydan, & Aykanat, 2023). Poria brown rot fungi, *Poria placenta* (Fr.) Lars. & Lombard (Mad-698-R) (Pop) was grown in malt agar media for two weeks in Petri dishes (90 mm diameter). The fungi virulence was tested using samples from *Pinus pinaster* (sapwood) and *Fagus sylvatica* wood. In total, 44 samples (around 10 mm × 10 mm × 5 mm) of various formulations were weighed, sterilized, and put in Petri dishes with fungi. The containers with samples were stored in a climate room at a temperature of 22 °C and 75 % relative humidity for 30 days. After that, all samples were cleaned and then were weighted for moisture content calculations. Then they were dried at a temperature of 70 ± 2 °C, for three days and weighed, and the weight loss was calculated.

2.3.10. Statistical analysis: Tukey's test

All the results were reported as mean ± standard deviation. One-way analysis of variance (ANOVA) and Tukey's test were used to determine the relevance in differences among the mean values at a 0.05 level of significance using Origin 2022 software.

3. Results and discussion

3.1. Analysis of the effect of $NaHCO_3$ and fillers on the aspect, apparent density, and foamability

The inspection of the photographs of the samples reported in Fig. 2 (a) highlighted that the presence of $NaHCO_3$ and fibers (type and concentration) had a strong effect on the appearance and expansion capability of the foams. The color of samples was characteristic of the filler used, samples filled with A-F400 were white while F fibers provided a brownish color, see fillers in Fig. S1 (a-b). The blowing agent sodium bicarbonate also induced a color change towards yellow, which could be associated with a partial dextrinization of starch (Chinnaswamy & Hanna, 1988; Jebalia et al., 2019). Moreover, this blowing agent generated more visible "super macro holes" or "nodules" on the surface in all the samples. The expansion capability of the samples is represented in Fig. 2 (a). Note that the expansion ratio is 1 when the sample does not suffer any volume change. The loss of water during the foaming process and the shrinkage of the starch could result in a final contraction of the sample and the negative value of the RS sample (Liu et al., 2023; Peng et al., 2022). It was clearly observed that fibers, long F fibers (3.4 cm) and 6 wt% of shorter A-F400 microfibers (2 mm), had a positive effect on the foam expansion, reaching values of 2 for samples containing flax fibers. This is because fibers can act as a skeleton during the retraction step, limiting the shrinkage (Liu et al., 2023; Peng et al., 2022). As expected, the addition of $NaHCO_3$ strongly enhanced the starch expansion acting as a blowing agent.

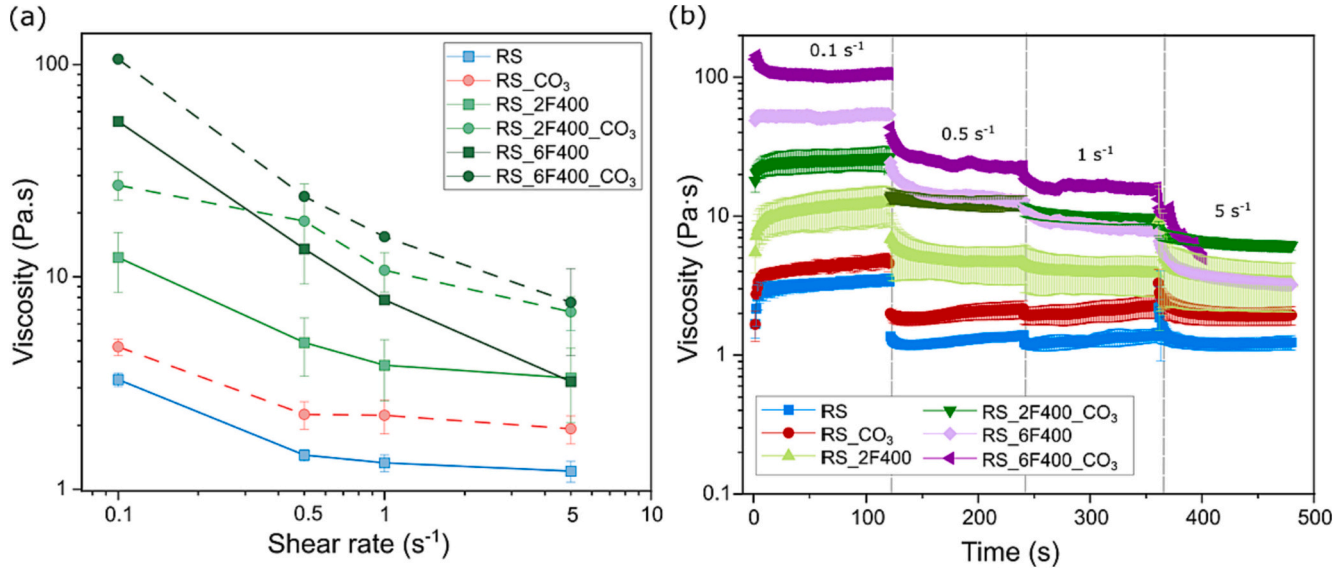

Fig. 3. (a) The flow curves of the pre-foaming samples, viscosity vs shear rate. The values of viscosities represented were taken at the end of the application of a given shear rate. (b) Viscosity vs time for each shear rate 0.1–5 s^{-1}. Note that these values may not reflect the steady-state viscosities.

The apparent density of samples represented in Fig. 2 (c) varied from 0.52 to 0.89 g/cm^3 depending on the sample. These values were comparable with other starch-cellulose foam composites reported by (Bénézet, Stanojlovic-Davidovic, Bergeret, Ferry, & Crespy, 2012; Soykeabkaew, Supaphol, & Rujiravanit, 2004), or even starch xerogels containing textiles-derived fibers (Négrier et al., 2023). Indeed, some materials qualified for external cushioning packaging, like kraft paper, are around 0.65 g/cm^3, indicating that the materials performed in this study could be suitable for this application (Peng et al., 2022). In general, the density of all starch samples reduced significantly with the addition of $NaHCO_3$ (represented as circles in Fig. 2 (c)). For example, the apparent density of the neat starch sample (RS) decreased from around 0.87 g/cm^3 to 0.58 g/cm^3 for RS_CO_3. Adding A-F400 did not significantly reduce the apparent density at any concentration, while foams containing 2 wt% of F (RS_2F) showed lower density with respect to RS (by 20 % less).

3.2. Study of the rheological characteristic of starch composites

Fiber-like fillers can usually have two opposite effects on the foaming process of a polymer matrix. On the one hand, fibers can favour the formation of vapour bubbles during the foaming process acting as a nucleating agent (Bergel et al., 2021; Duan et al., 2022; Tacha et al., 2023). This occurs due to the presence of micropores or voids in the polymer-filler interface, which provokes the migration of gas generation from the blowing agent to these regions. This effect usually increases with the concentration and smaller size of fibers (Zhou & Zhang, 2023; Zimmermann, da Silva, Zattera, & Campomanes Santana, 2017). On the other hand, these fillers can promote the increase of apparent viscosity of the initial formulation constituting a "mechanical network" around the cells, inhibiting the pore growth and leading to a denser morphology (Bergel et al., 2021; Négrier et al., 2023; Peng et al., 2022; Soykeabkaew et al., 2015). Therefore, the evaluation of the influence of each component (i.e., presence of fiber or $NaHCO_3$, type of fiber) on the overall viscosity was analyzed in terms of the rheological behaviour of the starch suspension (before the MW irradiation). Fig. 3 (a) exhibits the

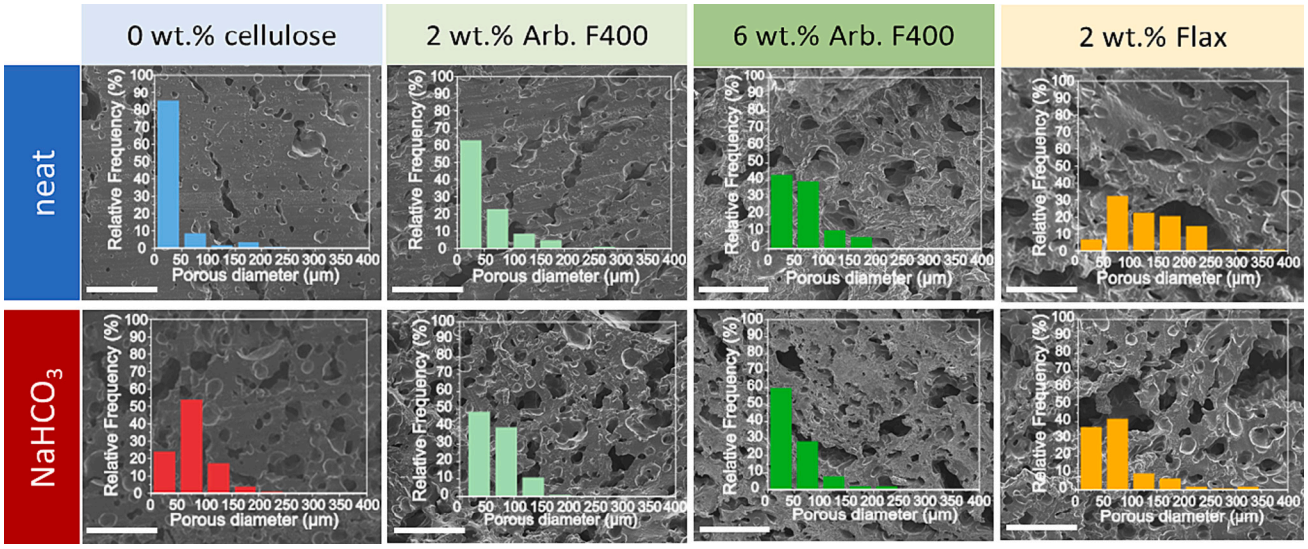

Fig. 4. The cross-section SEM images and histograms of the porous size distribution of all the samples. The scale bar corresponded to 50 μm.

Table 2
Values of porosity, cell density, and average cell size of the starch foam composites.

Sample	Average cell size (μm)	Porosity (%)	Cell density (cell/cm^3 ·10^6)
RS	39 ± 36	41	1.4
RS_CO_3	76 ± 39	61	17.4
RS_2F400	55 ± 45	40	3.0
RS_2F400_CO_3	71 ±42	51	10.9
RS_6F400	66 ± 43	46	3.2
RS_6F400_CO_3	54 ± 42	55	10.6
RS_2F	97 ± 56	54	3.6
RS_2F_CO_3	79 ± 63	65	9.6

values of viscosity at different shear rates for each sample. Results revealed that the viscosity globally decreased with increasing the shear rate, indicating a shear thinning behaviour of the samples. As expected, the viscosity increased with the content of fiber. The higher viscosities at the low shear rate observed when A-F400 fiber was added could be interpreted as a consequence of the apparition of an H-bonding network between the cellulose fiber and the starch, as already reported by (Peng, Ren, Zhong, Cao, & Sun, 2011; Xie, Yan, Yuan, Sun, & Huo, 2013). However, interestingly, the shear thinning behaviour was more pronounced when the concentration of fibers increased (see curves RS_2F400 and RS_6F400). The decrement of viscosity when the shear rate increased could be related to the disruption of the linkages between the starch particles and fibers, as well as with the alignment of fiber along the flow (Greene & Wilkes, 1995; Ou, Xie, Wolcott, Yuan, & Wang, 2014). The alignment of the fibers is an effect commonly observed in fiber-filled polymers, such as polypropylene, polycarbonate, or nylon 6/6 (Greene & Wilkes, 1995). However, this decrement was less significant in samples filled with $NaHCO_3$, regardless of the concentration of fiber. This could be associated with an increment of H-bonding interaction between the fibers and starch, due to the pulping effect of the $NaHCO_3$, which hampered the alignment of the fibers (Peng et al., 2011; Zhang et al., 2021). The higher viscosity observed in starch samples loaded with fibers could have provided good dimensional stability to foams preventing the shrinkage after the foam expansion, see Fig. 2(b).

Fig. 3 (b) displays the viscosity versus time at the different shear rates applied. All samples exhibited a complex behaviour, displaying an unstable viscosity after 2 min of shear (e.g., shear rates 0.5 and 1 s^{-1} for RS and RS_CO_3 systems). This instability at a constant shear rate was probably due to the thixotropic behaviour of the suspensions, which was not surprising at such particle concentration (starch and fiber beyond 50 wt%) (Wang et al., 2022). It is important to note that the high length of F fibers hindered the measurement of viscosity for this set of samples, and the noisy signal obtained at 5 s^{-1} for RS_6F400_CO_3 was associated with the apparition of strong heterogeneities in the material, ejected in part from the geometry.

3.3. Inner morphology of the foam composite

Fig. 4 displays the cross-section images of all the samples with the corresponding pore's diameter diagrams (inset figure). In all cases, the foams displayed very non-uniform porosity, with a pores size distribution ranging from 1 μm to 400 μm, as a result of the presence of different porogenic molecules and blowing agents involved in the foaming process (i.e., water and CO_2). All micrographs displayed cracks and holes that suggested a highly interconnected cellular structure, as observed in similar works (Bergel et al., 2021; Lopez-Gil et al., 2015).

The values of cell density (cell/cm^3 x 10^6), average cell size (μm), and porosity are reported in Table 2. The results of the cell density (cell/cm^3 x 10^6) and porosity revealed the positive effect of the $NaHCO_3$ and fibers on increasing the number of pores on the starch matrix, acting as a blowing and nucleating agent, respectively. In comparison, the results of cell density were slightly greater than those presented in polycarbonate foams filled with long carbon fiber and short glass fiber (Zhou & Zhang, 2023). The lower apparent density of cellulosic-fiber composites was also associated with the increment of the size of the pores observed in these samples. Especially in samples filled with F, up to three times

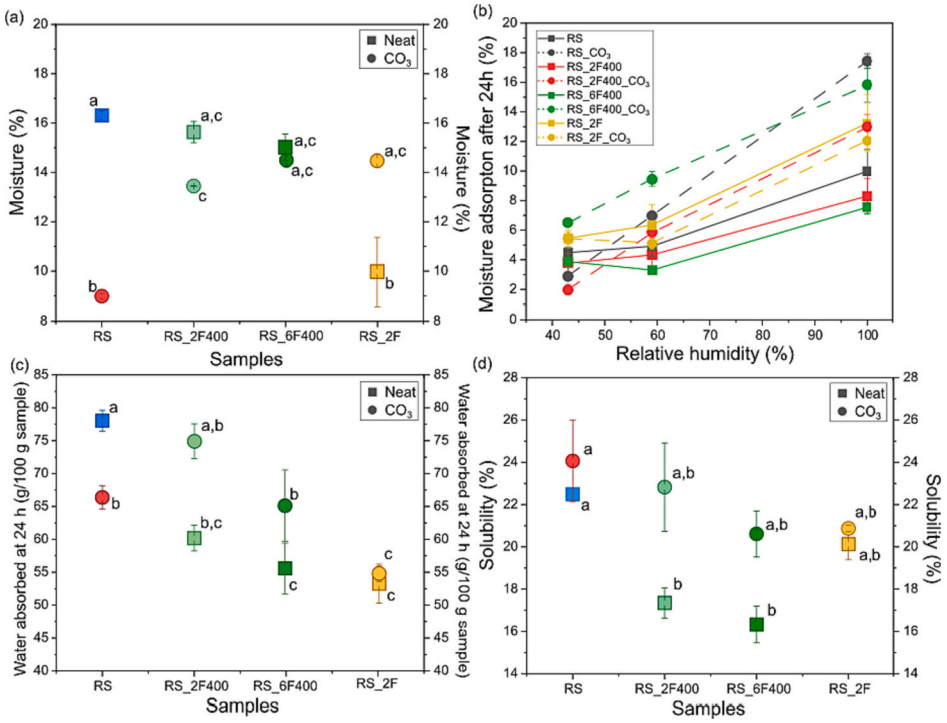

Fig. 5. The values of (a) moisture (b) water adsorbed after 24 h in fixed RH%, (b) liquid water adsorbed after immersion for 24 h and (c) water-soluble fraction of all the neat samples, represented as squares, and samples treated with $NaHCO_3$, represented as circles. The same letters indicate nonsignificant differences among the results according to Tukey's test ($p < 0.05$).

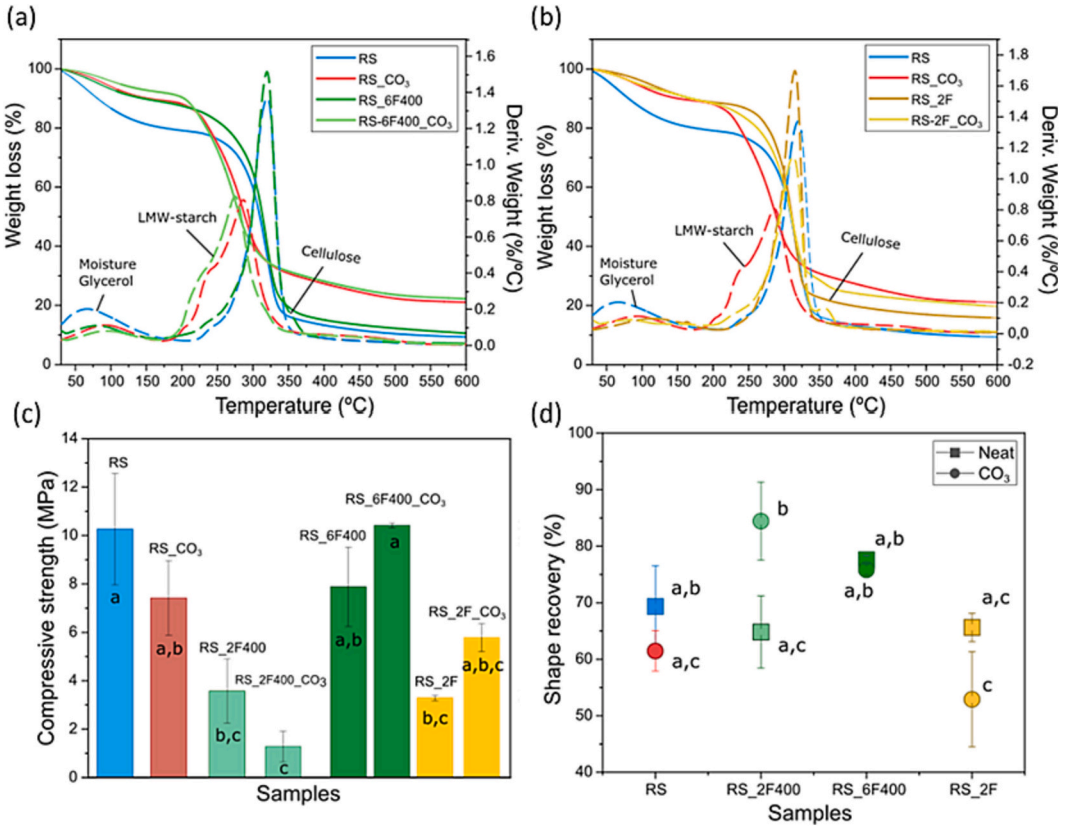

Fig. 6. TG and DGT curves and thermal values of RS samples filled with (a) A-F400 and (b) F fibers. (c) The compressive strength values for each sample. (d) The shape recovery values. The same letters indicate nonsignificant differences among the results according to Tukey's test ($p < 0.05$).

values displayed by neat foams for RS_2F sample, 39 μm in RS against 97 μm in RS_2F, denoting the positive effect of the length of the fiber on the pore growing. (Peng et al., 2022) reported that long microfibers (> 1 mm) enhance the formation of bigger bubbles due to the better capability of conducting the stress after the bubble disruption and retraction of the starch. (Zimmermann et al., 2017) discussed the high importance of the aggregation of fibers, which increases with content and length, in the formation of larger cells. This occurs because the gas from the blowing agent tends to migrate to the least resistant region and propagates its growth from this point. Therefore, the notable reduction of pore size when these samples were treated with $NaHCO_3$ could indicate a better dispersion of the fibers through the matrix.

As explained previously, the viscosity of the batter is also highly important for the foaming process because it limits the expansion of the bubble (Bergel et al., 2021; Peng et al., 2022). A major intermolecular interaction between the fibers and starch with the pulping effect of $NaHCO_3$, which resulted in an increment of hydroxyl groups available, resulted in an increment of the viscosity (see Fig. 3) (Liu et al., 2023). The effect of the pulping treatment on the cellulosic fibers was evidenced with microscopy, thermogravimetric analysis, and infrared spectroscopy of Figs. S4 and S5 in Supporting information. Fibers were easily appreciable and appeared well impregnated in the starch matrix in the micrographs reported in Fig. S6 of Supporting information, evidencing the good compatibility between the two components and the eventual attaching of the starch after retraction (Lopez-Gil et al., 2015; Prachayawarakorn, Ruttanabus, & Boonsom, 2011). It's worth noticing that the thermal degradation of fibers started around 200 °C, revealing that the temperature could damage the fiber features, such as the extrusion with polymers with higher processing temperatures, like polypropylene (PP) and polylactic acid (PLA) (Peltola, Pääkkönen, Jetsu, & Heinemann, 2014; Völtz et al., 2023; Wei et al., 2023). Moreover, extrusion can lead to the breakage of long fibers or degrading, while microwave ensures the preservation of the long fibers' morphology after the processing (Peltola et al., 2014; Rodríguez-Fabià, Zarna, & Chinga-Carrasco, 2023; Zhou & Zhang, 2023). Finally, as observed in other starch foams loaded with fibers processed through similar methods (Lopez-Gil et al., 2015; Rodríguez-Fabià et al., 2023), fibers were not oriented inside the matrix.

3.4. Water resistance properties

The results of the moisture content of neat and composite foams are represented in Fig. 5 (a). Neat starch foam exhibited around 17 % moisture content, slightly superior to other starch composites reported in the literature (Bergel et al., 2021; Quilez-Molina et al., 2023). The addition of fibers reduced the moisture content in starch foams, likely due to the formation of hydrogen bonds between the hydrophilic filler and the starch matrix, preventing the interaction between the OH of starch molecules with water moisture (Bergel et al., 2021; Quilez-Molina, Chandra Paul, Merino, & Athanassiou, 2022). The bleaching effect of $NaHCO_3$ resulted in an increment of moisture sensitivity of cellulosic-starch composites, especially in flax fibers ($RS\_2F\_CO_3$), see SEM images and infrared spectra Fig. S5 (f) of Supporting information. The moisture adsorption of the samples after exposure for 24 h to different humidity environmental conditions is represented in Fig. 5 (b). As expected, the moisture adsorption increased with the relative moisture environment, although a decrease in adsorption was observed with the incorporation of filler. The increment of moisture adsorption in samples treated with $NaHCO_3$ was primarily linked to the superior porosity, which contributed to increasing the available surface for water interaction (Bergel et al., 2021).

Noticeably, the starch foams loaded with 6 wt% of A-F400 (RS_6F400) displayed a moisture adsorption value of 4 % after being exposed for 24 h to 100 % humidity, which highlights the greater

stability of the composite to outdoor applications. The values of the water adsorption (g water/ 100 g of sample) of the foams after 24 h are represented in Fig. 5 (c). These results showed the remarkable positive effect of the fibers in improving the water resistance in samples, which increased with the fiber content and especially with F. As observed above, these results were associated with the interaction between cellulose and starch matrix, and with the hydrophobic nature of flax (Bergel et al., 2021; Prabhakar et al., 2017; Prachayawarakorn et al., 2011). The values obtained in samples without $NaHCO_3$ (below 60 g/100 g sample) were quite below with respect to other thermoplastic starch foams containing 1, 3, and 5 wt% of cotton fibers, which showed 68–80 g of water/100 g solid (Bergel et al., 2021). Interestingly, these results were comparable with extruded starch-based foams combined with a petroleum-derived polymer (polyvinyl alcohol, PVA) with different hydrolysis degrees (Liu et al., 2023). As observed in Fig. S7 of Supporting information, these differences are remarkable from the first 10 min of water adsorption, which reached a maximum of 55 g water/100 g sample for RS_6F400_CO_3, and which was entirely accomplished within the first hour. This effect was associated with the sample's open-cell porosity, which facilitated the entrance, permeation and diffusion of the water through the microstructure (Bergel et al., 2021). Fig. 5 (d) displays the values of the water solubility fraction of samples after 24 h of water immersion. As a general rule, the addition of fibers strengthened the water resistance of the foam composites by reducing the water solubility fraction by hydrogen bond interaction. The higher solubility of samples treated with $NaHCO_3$ was associated with the LMW (low molecular weight)-starch molecules due to the starch dextrinization with a superior water solubility (Bergel et al., 2021; Quilez-Molina et al., 2023).

In summary, results showed that the treatment with $NaHCO_3$ had a negative effect on the water sensitivity properties of the cellulosic-starch composite foams, while the filler improved the resistance of starch by creating a hydrogen network with the matrix. Overall, the sample RS_6F400 was shown to provide the best water-resistance features, especially in terms of water adsorption and solubility.

3.5. Thermal and mechanical properties

In Fig. 6 (a-b), the thermal degradation curve of the neat starch (colored in blue) was shown to degrade in two main steps. The first degradation step occurred below 200 °C associated with the volatilization of moisture and glycerol, while the main mass loss step (60 %), associated with the decomposition of the starch, occurred in a range of 250–360 °C, with the maximum decomposition rate at 320 °C (Prabhakar et al., 2017). Fig. 6 (a) shows that the addition of A-F400 in 6 wt% did not modify the thermal degradation of starch (320 °C), however, the thermal profiles exhibited an important decrement of moisture loss, which indicated the cellulosic fibers are able to reduce the absorption of moisture. The low amount of moisture is very important in terms of material stability and applicability (Liu et al., 2023; Soykeabkaew et al., 2015). Noticeably, the effect of the treatment with $NaHCO_3$ was observed in the thermal profile of RS_CO_3 and RS_6F400_CO_3 samples. Contrary to the neat samples, the thermal degradation occurred in two steps at lower temperatures: a new peak at about 237 °C, with a mass loss of 12 %, and the main degradation peak downshifted to 240 °C (about 10 °C less). These thermal patterns were associated with the presence of low-molecular-weight (LMW) starch molecules (i.e., dextrins) that decompose at a lower temperature due to the basic hydrolytic conditions in presence of $NaHCO_3$ (pH ∼ 8.5), coupled with the microwave irradiation, (Chen et al., 2019; Quilez-Molina et al., 2023; Zuo et al., 2014). The thermal curves of samples containing F fibers displayed in Fig. 6 (b) revealed that F slightly reduced the thermal resistance of the starch, exhibiting the maximum degradation peak at 315 °C, 5 °C below the neat RS sample. Their content of hemicellulose, which presents weaker thermal stability, led to composites with lower thermal resistance (Merino & Athanassiou, 2023; Quilez-Molina, Chandra Paul, et al., 2022). Interestingly, the peak related to the LWM-starch is rather visible in RS_2F_CO_3, which suggested that F fibers protected starch from degradation. Similar to A-F400 fibers, the addition of F fibers reduced the moisture content of starch composites. The increment of residual char was associated with the presence of Na_2CO_3 resulting from the thermal decomposition of $NaHCO_3$, as observed with other composites containing inorganic additives (Zhang et al., 2012).

In general, the chemical composition of rice starch, based on low content of amylose biopolymer (∼ 25 %) and rich in amylopectin (∼ 75 %), makes this kind of starch quite friable and brittle (Prachayawarakorn et al., 2011). The addition of cellulosic fibers as reinforcement has been a widely easy method employed to improve this property (Peltola et al., 2014; Rodríguez-Fabià et al., 2023). The compression curve of the RS_2F400, selected as a representative example, is displayed in Fig. S8. The compression stress-strain curve showed the typical profile of hard foams, which consisted of a first linear elasticity region (up to strain of 5–10 %), followed by a slight plateau of deformation, and a final zone where the collapse of the closed cell structure and foam densification occurs (Kim et al., 2021; Miranda-Valdez et al., 2023). However, the profile of the compression stress-strain curves strongly depends on the polymeric cell structure. Generally, in high-density polymeric foams, such as the materials presented in this work, the stress gradually increases beyond the elastic zone up to the cell collapse (Kim et al., 2021). Similar compression curves have been also observed in other starch-based composite foams loaded with sisal fibers (5 mm) (Ji et al., 2021). Fig. 6 (a) displays the compressive strength of the samples with 70 % compression. Results showed that $NaHCO_3$ contributed to the reduction of foam rigidity in RS_CO_3 and RS_2F400_CO_3, in comparison with untreated samples. However, the mechanical strength was improved in RS_6F400_CO_3 and RS_2F_CO_3. This result was associated with the effect of $NaHCO_3$ in modifying the cell size, smaller cell size is related to better mechanical properties (Kim et al., 2021; Zhou & Zhang, 2023). For the latter samples, $NaHCO_3$ improved the fibers' dispersion after the pulping with $NaHCO_3$, which reduced the formation of agglomerates and increased the hydrogen bonding network (Bergel et al., 2021; Bernaoui, Lebrun, & Ruiz, 2022; Rodríguez-Fabià et al., 2023). Therefore, the mechanical properties of starch foams were mainly subjected to their microstructure (i.e., porosity) and fiber dispersion.

The results of compressive strength obtained for some of these composites greatly exceeded, up to 3 times, the values exhibited in starch foams reinforced with sisal fiber of 1 mm, 5 mm, and 10 mm loaded in 40 % (∼ 2 MPa) (Peng et al., 2022). The shape recovery (%) is represented in Fig. 6 (b). These results highlighted the capability of the samples to recover the original shape after the compression test, which is strongly dependent on the friability of the cells (Kim et al., 2021). Overall, all samples showed relatively good recovery properties after compressions up to 70 % of the original height, showing a minimum of 52 % for RS_2F_CO_3 and a maximum of 84 % for RS_2F400_CO_3. Overall, samples filled with 6 wt% of A-F400 (with or without $NaHCO_3$) displayed better shape recovery, which indicated that these fiber's efficiency prevented the collapse of the cells at high compression loadings. Interestingly, the plasticizing effect of water could have positively contributed to the high value of recovery obtained in these foams (Mali, Debiagi, Grossmann, & Yamashita, 2010; Soykeabkaew et al., 2004).

3.6. Biodegradation

Evaluating the biodegradability of samples is highly important for the application of these eco-friendly composites in the environment. A biodegradation test was carried out with the brown-rot fungus *Poria Placenta*, ubiquitously found in nature, which degrades cellulose (preferentially) and lignin (Can et al., 2023).

The biodegradability of the dried porous samples ($1 \times 1 \times 0.5$ cm^3) was tested and compared with dried tablets of neat dry sintered starch-dense powder, A-F400, and F, as well as wooden pieces of pine and beech (1x1x0.5 cm^3), used as references. Each replicate of the sample

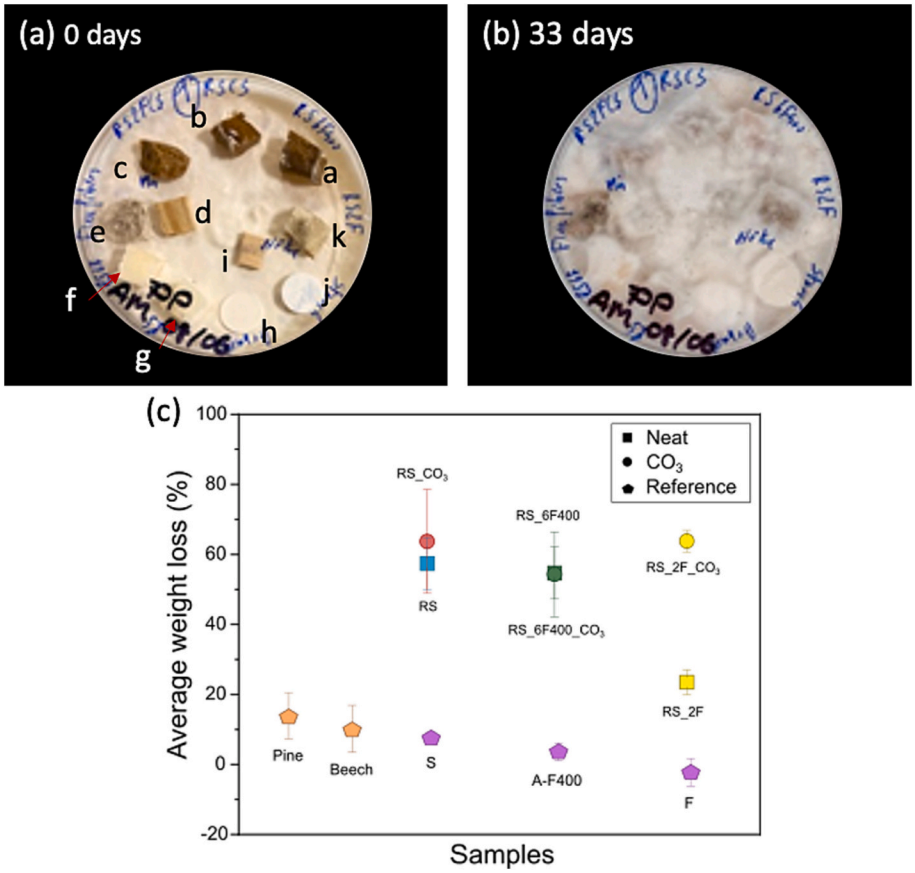

Fig. 7. The photograph of the samples (a) at the beginning and (b) at the end of the biodegradability test. The samples were marked as a: RS_6F400_CO_3, b: RS_CO_3, c: RS_2F_CO_3, d: pine, e: flax fibers, f: RS_6F400, g: RS, h: A-F400 fibers, i: beech, j: starch powder, and k: RS_2F. (c) The average weight loss of specimens after 33 days of experiment.

and reference was placed in the same Petri dish with the same sample's repartition, see the photograph of Fig. 7 (a). 4 Petri dishes of malt-agar and inoculated fungus were incubated (25 °C, 70 % RH) for 33 days. As observed in Fig. 7 (a-b), at the end of the experiment the colony of fungi greatly expanded to completely cover the samples. During this process, the fungi grew on the surface of the foam, decomposing and fragmenting the sample to obtain the nutrients (Can et al., 2023; Zhang et al., 2022). The results of the biodegradability test are displayed in Fig. 7 (c). The first global observation is that a period of 33 days was quite enough to degrade most of the starch-based foams/composites to a large extent (> 50 wt%), overcoming greatly the degradation of the wooden pieces of pine and beech, and the neat-sintered reference tablets. This high biodegradation rate was comparable with the degradation in the soil of other starch foams filled with fibers, such as the cassava starch foams filled with 10 wt% of sugarcane fibers reported by (Ketkaew et al., 2018). Generally, the capability of the microbe to degrade matter depends on the nature of the material (hydrophilicity, and crystallinity), the humidity conditions, and the compacity of the material (porosity) (Prabhakar et al., 2017). However, it can be assumed that the effect of porosity was predominant, while the influence of starch material was the second trigger (comparing porous starch to dense starch). Table S1 relates the highest mass losses to the highest porosities; the most porous (> 40 %) being the most degraded (> 60 %). Note that densified starch or densified cellulose fibers needed a longer time to degrade.

In the SEM pictures of the biodegraded samples reported in Fig. S9 (a-d) of Supporting information, the mycelium and fungus elements were easily distinguished on all the samples. The ubiquitous expansion of the mycelium overall the surface underlined the good adhesion and affinity with the samples. Moreover, the apparition of holes randomly distributed on the samples (marked with red arrows in Fig. S10), noted the degradation of the organic matter (Can et al., 2023). The lack of these holes on wood pieces might confirm the lower degradation rate in comparison with starch-based samples.

3.7. Sustainability study: greenhouse gas (GHG) emissions

As introduced before, this project is conceived with the aim of employing fiber waste from the textile industry as a cellulosic filler. Therefore, separated cotton clothing fibers, in a size around 2 mm and without dyes, (such as commercial A-F400 fibers) were considered as the filler to obtain the sample that presented the best properties, RS_6F400. Moreover, it will only be considered the GHG generated during the production and treatment of the reagents, as well as during the sample fabrication.

According to the study reported by (Espinoza Pérez et al., 2022), the treatment of recycling textile fibers generated about 1142.12 kg CO_{2eq}/ton of fiber. Therefore, for this formulation, the fiber processing corresponded to 55 kgCO_{2eq} per ton of foam composite. Moreover, the GHG emissions associated with the extraction processing of the crop to obtain the starch polymer were around 105–150 kg CO_{2eq}/t, which can vary with the crop and producing country (Tran et al., 2015). It's important to consider that the values of net GHG emissions for other non-biodegradable petroleum-based plastics like polypropylene (PP) and low-density polyethylene (LDPE) are close to 2000 kg CO_{2eq}/t in both polymers (Broeren, Kuling, Worrell, & Shen, 2017; Pang, Pun, Chow, & Ishak, 2014). This corresponds to a total of 81 kgCO_{2eq} per ton of RS_6F400 produced. The plasticizers usually have GHG emissions of 1950 kg CO_{2eq}/ton (Broeren et al., 2016; Pang et al., 2014), which corresponds to 390 kgCO_{2eq} per ton of the present formulation. The values of carbon intensity (CI) of electricity consumed at low voltage

Table 3
Values of GHG emissions for different polymer composites.

Material	Filler (wt%)	Fabrication method	$kgCO_{2eq}$/ton composite	Reference
Starch foamed composites	6 wt% Arbocell® A-F400 fibers (2 mm)	Microwave irradiation	526	This work
PP composites	20 wt% Talc	Extrusion + Thermoforming	4430	(Pang et al., 2014)
PLA/ TPS	–	Extrusion + Thermoforming	1000	(Broeren et al., 2017)
PP composites	30 wt% cotton fiber	Extrusion + Thermoforming	555	(Völtz et al., 2023)
PP composites	30 wt% glass fiber	Extrusion + Thermoforming	~ 6700	(Boland et al., 2016)
PP composites	40 wt% kenaf fiber	Extrusion + Thermoforming	~ 5300	(Boland et al., 2016)

Abbreviations: PLA = polylactic acid; TPS = Thermoplastic starch; PP = polypropylene. Note that the values calculated were approximative. Some costs, such as the raw material transportation or use phase, were not considered in this work. This could have influenced the difference in emissions concerning other works whose aim was only the study of the life cycle assessment of the composites.

found elsewhere (Scarlat, Prussi, & Padella, 2022), corresponded to 0.98 gCO_2/kWh in France in 2019. Considering this data, the MW processing produced 0.81 $kgCO_{2eq}$ per ton of material fabricated. The sum of all these factors resulted in a total of around 526 $kgCO_{2eq}$ per ton of the RS_6F400 foam. Interestingly, the GHG emitted for the material production was comparable with textile fibers (without recycling process) combined with cheap petroleum-based polymer PP through extrusion reported by (Völtz et al., 2023), or better than other polymer composites reported in Table 3. Moreover, it's important to highlight the potential environmental benefits, in terms of biobased feedstock and excellent biodegradability in natural conditions (see biodegradability test). The latter is greatly interesting for avoiding additional costs related to waste management or recycling, but also for reducing environmental impact due to the calcination of plastics. For fibers, the calcination of textiles in landfills corresponds to around 0.423 kg CO_2eq/kg, while plastic wastes generate around 5.1 tons of CO_2 every year (Correa, Montalvo-Navarrete, & Hidalgo-Salazar, 2019; Espinoza Pérez et al., 2022). To conclude, it's worth noticing that the plasticizer was the component that contributed more to the GHG emission, which underlined the importance of searching for new plasticizers for reducing the carbon footprint in future works.

4. Conclusion

"All polysaccharide" composite foams from cellulosic fibers resources, with lower density, good water, and mechanical resistance, and excellent degradability through a sustainable and low-cost process were successfully achieved. Sodium bicarbonate, with a double role as a blowing and pulping agent, was shown to be critical to defining the final properties of the starch foams by reducing the apparent density of foams, but also by improving the dispersion and interaction with the matrix (i.e., removing non-cellulosic carbohydrates). As a result, the mechanical properties of the fiber's composites pulped with $NaHCO_3$ showed better thermal and mechanical resistance, the latter was associated with the increasing hydrogen bond network and reduction of fibers' agglomerates, which otherwise promoted bigger pores with poorer mechanical features. However, the higher porosity reached with $NaHCO_3$ was shown to have a negative effect on the water resistance properties of foams. Overall, the sample RS_6F400 (i.e., 6 wt% pure cellulose fibers) showed the best properties in terms of low density, mechanical, thermal, and water resistance properties, as well as excellent biodegradability. However, the pulping treatment remarkably improved the properties of starch composites containing raw textile flax fibers, which suggests that this treatment could be employed for fabricating sustainable composites with fibers that present similar chemical features.

In conclusion, most starch foams containing cellulosic fibers exhibited excellent biodegradability in contact with the fungus *Poria Placenta*, losing >50 % of the initial weight. In addition to their good functionalities, these composites exhibited a better environmental performance than analogous systems. The foams can be designed to give a second life cycle to industrial waste (textile fibers), as assessed by a calculation of low GHG emissions.

CRediT authorship contribution statement

Ana Isabel Quilez-Molina: Writing – original draft, Visualization, Methodology, Investigation, Formal analysis, Data curation, Conceptualization. **Jean François Le Meins:** Writing – review & editing, Validation, Data curation. **Bertrand Charrier:** Writing – review & editing, Validation, Data curation. **Michel Dumon:** Writing – review & editing, Supervision, Project administration, Conceptualization.

Declaration of competing interest

The authors declare that they have no known competing financial interests or personal relationships that could have appeared to influence the work reported in this paper.

Data availability

Data will be made available on request.

Acknowledgements

The authors gratefully acknowledge Jean-Marc Tallon, from the Department of Science et Genie des Matériaux (IUT Bordeaux) for the technical assistance in SEM observations, as well as Jean-Eudes Maigret, from Laboratory BIA at INRAE Nantes for measurement of the amylose content of rice starch by a calorimetry analysis. Finally, we thank the Spanish Ministry of Universities and the Next Generation EU-Recovery for funding the post-doctoral grant "Margarita Salas" of A. Q.

Appendix A. Supplementary data

Supplementary data to this article can be found online at https://doi.org/10.1016/j.carbpol.2023.121743.

References

Adu, C., Jolly, M., & Thakur, V. K. (2018). Exploring new horizons for paper recycling: A review of biomaterials and biorefinery feedstocks derived from wastepaper. In , *Vol. 13. Current opinion in green and sustainable chemistry* (pp. 21–26). Elsevier B.V.. https://doi.org/10.1016/j.cogsc.2018.03.003

Alam, M. N., & Christopher, L. P. (2017). A novel, cost-effective and eco-friendly method for preparation of textile fibers from cellulosic pulps. *Carbohydrate Polymers, 173*, 253–258. https://doi.org/10.1016/j.carbpol.2017.06.005

Almeida, J. A., Oliveira, A. S., Rigoti, E., Neto, J. C. D., de Alcântara, & Pergher, S. B. C. (2019). Design of solid foams for flame retardant based on bionanocomposites systems. *Applied Clay Science, 180*. https://doi.org/10.1016/j.clay.2019.105173

Bénézet, J. C., Stanojlovic-Davidovic, A., Bergeret, A., Ferry, L., & Crespy, A. (2012). Mechanical and physical properties of expanded starch, reinforced by natural fibres. *Industrial Crops and Products, 37*(1), 435–440. https://doi.org/10.1016/j.indcrop.2011.07.001

Bergel, B. F., Araujo, L. L., & Santana, R. M. C. (2021). Effects of the addition of cotton fibers and cotton microfibers on the structure and mechanical properties of starch foams made from potato starch. *Carbohydrate Polymer Technologies and Applications, 2*. https://doi.org/10.1016/j.carpta.2021.100167

Bernaoui, A., Lebrun, G., & Ruiz, E. (2022). High performance natural fiber composites from mat and UD flax reinforcements backed with a mat binder: A study of mat fiber surface fibrillation. *Composites Part A: Applied Science and Manufacturing, 160*, Article 107064. https://doi.org/10.1016/j.compositesa.2022.107064

Boland, C. S., De Kleine, R., Keoleian, G. A., Lee, E. C., Kim, H. C., & Wallington, T. J. (2016). Life cycle impacts of natural fiber composites for automotive applications: Effects of renewable energy content and lightweighting. *Journal of Industrial Ecology, 20*(1), 179–189. https://doi.org/10.1111/jiec.12286

Broeren, M. L. M., Kuling, L., Worrell, E., & Shen, L. (2017). Environmental impact assessment of six starch plastics focusing on wastewater-derived starch and additives. *Resources, Conservation and Recycling, 127*, 246–255. https://doi.org/10.1016/j.resconrec.2017.09.001

Broeren, M. L. M., Molenveld, K., van den Oever, M. J. A., Patel, M. K., Worrell, E., & Shen, L. (2016). Early-stage sustainability assessment to assist with material selection: A case study for biobased printer panels. *Journal of Cleaner Production, 135*, 30–41. https://doi.org/10.1016/j.jclepro.2016.05.159

Can, A., Tomak, E. D., Ermeydan, M. A., & Aykanat, O. (2023). Synergic effect of basalt/wood fiber reinforced polylactic acid hybrid biocomposites against fungal decay. *European Polymer Journal, 112246*. https://doi.org/10.1016/j.eurpolymj.2023.112246

Chen, F., Xie, F., Liu, P., & Chen, P. (2019). Structure, thermal stability and suspension rheological properties of alcohol–alkali-treated waxy rice starch. *International Journal of Biological Macromolecules, 134*, 397–404. https://doi.org/10.1016/j.ijbiomac.2019.05.009

Chen, F. L., Ma, C. M., Dou, X. L., Fan, J., Yang, Y., He, Y. Y., … Zhang, N. (2022). Preparation and Physicochemical and Structural Properties of Broken Rice-Based Reconstituted Rice Produced by Extrusion Puffing Technology. *ACS Food Science and Technology, 2*(12), 1921–1928. https://doi.org/10.1021/acsfoodscitech.2c00281

Chen, H., Yu, Y., Zhong, T., Wu, Y., Li, Y., Wu, Z., & Fei, B. (2017). Effect of alkali treatment on microstructure and mechanical properties of individual bamboo fibers. *Cellulose, 24*(1), 333–347. https://doi.org/10.1007/s10570-016-1116-6

Chinnaswamy, R., & Hanna, M. A. (1988). Expansion, color and shear strength properties of com starches extrusion-cooked with urea and salts. *Starch - Stärke, 40*(5), 186–190. https://doi.org/10.1002/star.19880400507

Correa, J. P., Montalvo-Navarrete, J. M., & Hidalgo-Salazar, M. A. (2019). Carbon footprint considerations for biocomposite materials for sustainable products: A review. In , *Vol. 208*. *Journal of cleaner production* (pp. 785–794). Elsevier Ltd.. https://doi.org/10.1016/j.jclepro.2018.10.099

Dong, Z., Li, N., Chu, T., Ding, J., Zhang, J., & Dong, A. (2022). High-quality natural fibers from cotton stalk bark via limited alkali penetration and simultaneous accelerated temperature rise. *Materials, 15*(2). https://doi.org/10.3390/ma15020422

Duan, Q., Zhu, Z., Chen, Y., Liu, H., Yang, M., Chen, L., & Yu, L. (2022). Starch-based foams nucleated and reinforced by polysaccharide-based crystals. *ACS Sustainable Chemistry and Engineering, 10*(6), 2169–2179. https://doi.org/10.1021/acssuschemeng.1c07738

Escamilla-Pérez, A. M., Beda, A., Simonin, L., Grapotte, M. L., Le-Meins, J. M., & Matei Ghimbeu, C. (2023). Biopolymer-Based Hard Carbons: Correlations between Properties and Performance as a Na-Ion Battery Anode. *ACS Applied Energy Materials, 6*(14), 7419–7432. https://doi.org/10.1021/acsaem.3c00640

Espinoza Pérez, L. A., Espinoza Pérez, A. T., & Vásquez, Ó. C. (2022). Exploring an alternative to the Chilean textile waste: A carbon footprint assessment of a textile recycling process. *Science of the Total Environment, 830*. https://doi.org/10.1016/j.scitotenv.2022.154542

Foulk, J. A., Chao, W. Y., Akin, D. E., Dodd, R. B., & Layton, P. A. (2006). Analysis of flax and cotton fiber fabric blends and recycled polyethylene composites. *Journal of Polymers and the Environment, 14*(1), 15–25. https://doi.org/10.1007/s10924-005-8703-1

Georges, A., Lacoste, C., & Damien, E. (2018). Effect of formulation and process on the extrudability of starch-based foam cushions. *Industrial Crops and Products, 115*, 306–314. https://doi.org/10.1016/j.indcrop.2018.02.001

Gimeno, E., Moraru, C. I., & Kokini, J. L. (2004). Effect of xanthan gum and CMC on the structure and texture of corn flour pellets expanded by microwave heating. *Cereal Chemistry, 81*(1), 100–107. https://doi.org/10.1094/CCHEM.2004.81.1.100

Greene, J. P., & Wilkes, J. O. (1995). Steady-state and dynamic properties of concentrated fiber-filled thermoplastics. *Polymer Engineering & Science, 35*(21), 1670–1681. https://doi.org/10.1002/pen.760352103

Jebalia, I., Maigret, J. E., Réguerre, A. L., Novales, B., Guessasma, S., Lourdin, D., … Kristiawan, M. (2019). Morphology and mechanical behaviour of pea-based starch-protein composites obtained by extrusion. *Carbohydrate Polymers, 223*. https://doi.org/10.1016/j.carbpol.2019.115086

Ji, M., Li, F., Li, J., Li, J., Zhang, C., Sun, K., & Guo, Z. (2021). Enhanced mechanical properties, water resistance, thermal stability, and biodegradation of the starch-sisal fibre composites with various fillers. *Materials and Design, 198*. https://doi.org/10.1016/j.matdes.2020.109373

Juanga-Labayen, J. P., Labayen, I. V., & Yuan, Q. (2022). A review on textile recycling practices and challenges. *Textiles, 2*(1), 174–188. https://doi.org/10.3390/textiles2010010

Ketkaew, S., Kasemsiri, P., Hiziroglu, S., Mongkolthanaruk, W., Wannasutta, R., Pongsa, U., & Chindaprasirt, P. (2018). Effect of oregano essential oil content on properties of green biocomposites based on cassava starch and sugarcane bagasse for bioactive packaging. *Journal of Polymers and the Environment, 26*(1), 311–318. https://doi.org/10.1007/s10924-017-0957-x

Kim, J. D., Kim, J. H., Lee, D. H., Yeom, D. J., & Lee, J. M. (2021). Synthesis and investigation of cryogenic mechanical properties of chopped-glass-fiber-reinforced polyisocyanurate foam. *Materials, 14*(2), 1–18. https://doi.org/10.3390/ma14020446

Lee, S. Y., Eskridge, K. M., Koh, W. Y., & Hanna, M. A. (2009). Evaluation of ingredient effects on extruded starch-based foams using a supersaturated split-plot design. *Industrial Crops and Products, 29*(2–3), 427–436. https://doi.org/10.1016/j.indcrop.2008.08.003

Liu, F., Zhang, Y., Xiao, X., Cao, Y., Jiao, W., Bai, H., Yu, L., & Duan, Q. (2023). Effects of polyvinyl alcohol content and hydrolysis degree on the structure and properties of extruded starch-based foams. *Chemical Engineering Journal, 472*, Article 144959. https://doi.org/10.1016/j.cej.2023.144959

Lopez-Gil, A., Silva-Bellucci, F., Velasco, D., Ardanuy, M., & Rodriguez-Perez, M. A. (2015). Cellular structure and mechanical properties of starch-based foamed blocks reinforced with natural fibers and produced by microwave heating. *Industrial Crops and Products, 66*, 194–205. https://doi.org/10.1016/j.indcrop.2014.12.025

Lopresti, F., Botta, L., Scaffaro, R., Bilello, V., Settanni, L., & Gaglio, R. (2019). Antibacterial biopolymeric foams: Structure–property relationship and carvacrol release kinetics. *European Polymer Journal, 121*. https://doi.org/10.1016/j.eurpolymj.2019.109298

Mali, S., Debiagi, F., Grossmann, M. V. E., & Yamashita, F. (2010). Starch, sugarcane bagasse fibre, and polyvinyl alcohol effects on extruded foam properties: A mixture design approach. *Industrial Crops and Products, 32*(3), 353–359. https://doi.org/10.1016/j.indcrop.2010.05.014

Merino, D., & Athanassiou, A. (2023). Alkaline hydrolysis of biomass as an alternative green method for bioplastics preparation: In situ cellulose nanofibrillation. *Chemical Engineering Journal, 454*, Article 140171. https://doi.org/10.1016/j.cej.2022.140171

Mestres, C., Matencio, F., Pons, B., Yajid, M., & Fliedel, G. (1996). A rapid method for the determination of amylose content by using differential-scanning calorimetry. *Starch-Stärke, 48*(1), 2–6. https://doi.org/10.1002/star.19960480103

Miranda-Valdez, I. Y., Coffeng, S., Zhou, Y., Viitanen, L., Hu, X., Jannuzzi, L., … Alava, M. J. (2023). Foam-formed biocomposites based on cellulose products and lignin. *Cellulose, 30*(4), 2253–2266. https://doi.org/10.1007/s10570-022-05041-3

Mu, B., & Yang, Y. (2022). Complete separation of colorants from polymeric materials for cost-effective recycling of waste textiles. *Chemical Engineering Journal, 427*. https://doi.org/10.1016/j.cej.2021.131570

Naik, T. P., Singh, I., & Sharma, A. K. (2022). Processing of polymer matrix composites using microwave energy: A review. In , *Vol. 156*. *Composites part a: Applied science and manufacturing*. Elsevier Ltd.. https://doi.org/10.1016/j.compositesa.2022.106870

Négrier, M., El Ahmar, E., Sescousse, R., Sauceau, M., & Budtova, T. (2023). Upcycling of textile waste into high added value cellulose porous materials, aerogels and cryogels. *RSC Sustainability, 1*(2), 335–345. https://doi.org/10.1039/d2su00084a

Ou, R., Xie, Y., Wolcott, M. P., Yuan, F., & Wang, Q. (2014). Effect of wood cell wall composition on the rheological properties of wood particle/high density polyethylene composites. *Composites Science and Technology, 93*, 68–75. https://doi.org/10.1016/j.compscitech.2014.01.001

Pang, M. M., Pun, M. Y., Chow, W. S., & Ishak, Z. A. M. (2014). Carbon footprint calculation for thermoformed starch-filled polypropylene biobased materials. *Journal of Cleaner Production, 64*, 602–608. https://doi.org/10.1016/j.jclepro.2013.07.026

Peltola, H., Pääkkönen, E., Jetsu, P., & Heinemann, S. (2014). Wood based PLA and PP composites: Effect of fibre type and matrix polymer on fibre morphology, dispersion and composite properties. *Composites Part A: Applied Science and Manufacturing, 61*, 13–22. https://doi.org/10.1016/j.compositesa.2014.02.002

Peng, S., Li, F., Man, J., Li, J., Zhang, C., Ji, M., Li, J., & Wang, S. (2022). Enhancing the properties of starch-fiber foaming material by adjusting fiber length: The synergistic effect of macro-micro stress conduction. *Materials Today Communications, 33*, Article 104408. https://doi.org/10.1021/jf1036239

Peng, X. W., Ren, J. L., Zhong, L. X., Cao, X. F., & Sun, R. C. (2011). Microwave-induced synthesis of carboxymethyl hemicelluloses and their rheological properties. *Journal of Agricultural and Food Chemistry, 59*(2), 570–576. https://doi.org/10.1021/jf1036239

Pinto, J., Dumon, M., Pedros, M., Reglero, J., & Rodriguez-Perez, M. A. (2014). Nanocellular CO2 foaming of PMMA assisted by block copolymer nanostructuration. *Chemical Engineering Journal, 243*, 428–435. https://doi.org/10.1016/j.cej.2014.01.021

Poilâne, C., Cherif, Z. E., Richard, F., Vivet, A., Ben Doudou, B., & Chen, J. (2014). Polymer reinforced by flax fibres as a viscoelastoplastic material. *Composite Structures, 112*(1), 100–112. https://doi.org/10.1016/j.compstruct.2014.01.043

Prabhakar, M. N., Rehman Shah, A.u., & Song, J. I. (2017). Improved flame-retardant and tensile properties of thermoplastic starch/flax fabric green composites. *Carbohydrate Polymers, 168*, 201–211. https://doi.org/10.1016/j.carbpol.2017.03.036

Prachayawarakorn, J., Ruttanabus, P., & Boonsom, P. (2011). Effect of cotton fiber contents and lengths on properties of thermoplastic starch composites prepared from rice and waxy rice starches. *Journal of Polymers and the Environment, 19*(1), 274–282. https://doi.org/10.1007/s10924-010-0273-1

Quilez-Molina, A. I., Chandra Paul, U., Merino, D., & Athanassiou, A. (2022). Composites of thermoplastic starch and lignin-rich agricultural waste for the packaging of fatty foods. *ACS Sustainable Chemistry & Engineering.*. https://doi.org/10.1021/acssuschemeng.2c04326

Quilez-Molina, A. I., Heredia-Guerrero, J. A., Armirotti, A., Paul, U. C., Athanassiou, A., & Bayer, I. S. (2020). Comparison of physicochemical, mechanical and antioxidant properties of polyvinyl alcohol films containing green tealeaves waste extracts and discarded balsamic vinegar. *Food Packaging and Shelf Life, 23*. https://doi.org/10.1016/j.fpsl.2019.100445

Quilez-Molina, A. I., Mazzon, G., Athanassiou, A., & Perotto, G. (2022). A novel approach to fabricate edible and heat sealable bio-based films from vegetable biomass rich in pectin. *Materials Today Communications, 103871*. https://doi.org/10.1016/j.mtcomm.2022.103871

Quilez-Molina, A. I., Oliveira-Salmazo, L., Amezúa-Arranz, C., López-Gil, A., & Rodríguez-Pérez, M.Á. (2023). Evaluation of the acid hydrolysis as pre-treatment to enhance the integration and functionality of starch composites filled with rich-in-pectin agri-food waste orange peel. *Industrial Crops and Products, 205*, Article 117407. https://doi.org/10.1016/j.indcrop.2023.117407

Robin, F., Engmann, J., Pineau, N., Chanvrier, H., Bovet, N., & Valle, G. D. (2010). Extrusion, structure and mechanical properties of complex starchy foams. *Journal of Food Engineering, 98*(1), 19–27. https://doi.org/10.1016/j.jfoodeng.2009.11.016

Rodríguez-Fabià, S., Zarna, C., & Chinga-Carrasco, G. (2023). A comparative study of Kraft pulp fibres and the corresponding fibrillated materials as reinforcement of LDPE- and HDPE-biocomposites. *Composites Part A: Applied Science and Manufacturing, 173*. https://doi.org/10.1016/j.compositesa.2023.107678

Saed Hussein, M., Leng, T. P., Rahmat, A. R., Zainuddin, F., Cheow Keat, Y., Suppiah, K., & Salem Alsagayar, Z. (2019). The effect of sodium bicarbonate as blowing agent on the mechanical properties of epoxy. *Materials Today: Proceedings, 16*, 1622–1629. https://doi.org/10.1016/j.matpr.2019.06.027

Scarlat, N., Prussi, M., & Padella, M. (2022). Quantification of the carbon intensity of electricity produced and used in Europe. *Applied Energy, 305*. https://doi.org/10.1016/j.apenergy.2021.117901

Soykeabkaew, N., Supaphol, P., & Rujiravanit, R. (2004). Preparation and characterization of jute-and flax-reinforced starch-based composite foams. *Carbohydrate Polymers, 58*(1), 53–63. https://doi.org/10.1016/j.carbpol.2004.06.037

Soykeabkaew, N., Thanomsilp, C., & Suwantong, O. (2015). A review: Starch-based composite foams. In *, Vol. 78. Composites part a: Applied science and manufacturing* (pp. 246–263). Elsevier Ltd.. https://doi.org/10.1016/j.compositesa.2015.08.014

Tacha, S., Somord, K., Rattanawongkun, P., Intatha, U., Tawichai, N., & Soykeabkaew, N. (2023). Bio-nanocomposite foams of starch reinforced with bacterial nanocellulose fibers. *Materials Today: Proceedings, 75*, 119–123. https://doi.org/10.1016/j.matpr.2022.12.049

Tran, T., Da, G., Moreno-Santander, M. A., Vélez-Hernández, G. A., Giraldo-Toro, A., Piyachomkwan, K., … Dufour, D. (2015). A comparison of energy use, water use and carbon footprint of cassava starch production in Thailand, Vietnam and Colombia. *Resources, Conservation and Recycling, 100*, 31–40. https://doi.org/10.1016/j.resconrec.2015.04.007

Van Rijswijk, K., & Bersee, H. E. N. (2007). Reactive processing of textile fiber-reinforced thermoplastic composites - an overview. In *, Vol. 38, Issue 3. Composites Part A: Applied Science and Manufacturing* (pp. 666–681). https://doi.org/10.1016/j.compositesa.2006.05.007

Völtz, L. R., Berglund, L., & Oksman, K. (2023). Resource-efficient manufacturing process of composite materials: Fibrillation of recycled textiles and compounding with thermoplastic polymer. *Composites Part A: Applied Science and Manufacturing, 175*, Article 107773. https://doi.org/10.1016/j.compositesa.2023.107773

Wang, Y., Bai, Y., Ji, H., Dong, J., Li, X., Liu, J., & Jin, Z. (2022). Insights into rice starch degradation by maltogenic α–amylase: Effect of starch structure on its rheological properties. *Food Hydrocolloids, 124*. https://doi.org/10.1016/j.foodhyd.2021.107289

Wani, A. A., Singh, P., Shah, M. A., Schweiggert-Weisz, U., Gul, K., & Wani, I. A. (2012). Rice starch diversity: Effects on structural, morphological, thermal, and physicochemical properties-a review. In. *Comprehensive Reviews in Food Science and Food Safety, 11*(5), 417–436. https://doi.org/10.1111/j.1541-4337.2012.00193.x

Wei, Q. Y., Fang, Y. D., Sun, Z. B., Zeng, Y., Zhang, J., Lei, J., … Li, Z. M. (2023). Fabrication of PLA/CB composites with excellent electrical conductivity and stiffness-ductility balance based on coupling extensional stress with thermal field. *Composites Part A: Applied Science and Manufacturing, 169*. https://doi.org/10.1016/j.compositesa.2023.107516

Xie, Y., Yan, M., Yuan, S., Sun, S., & Huo, Q. (2013). Effect of microwave treatment on the physicochemical properties of potato starch granules. *Chemistry Central Journal, 7*(1), 1–7. https://doi.org/10.1186/1752-153X-7-113

Yildirim, N., Shaler, S. M., Gardner, D. J., Rice, R., & Bousfield, D. W. (2014). Cellulose nanofibril (CNF) reinforced starch insulating foams. *Cellulose, 21*(6), 4337–4347. https://doi.org/10.1007/s10570-014-0450-9

Yu, I. K. M., Chen, H., Abeln, F., Auta, H., Fan, J., Budarin, V. L., … Tsang, D. C. W. (2021). Chemicals from lignocellulosic biomass: A critical comparison between biochemical, microwave and thermochemical conversion methods. *Critical Reviews in Environmental Science and Technology, 51*(14), 1479–1532. https://doi.org/10.1080/10643389.2020.1753632

Zhang, J., Liu, B., Zhou, Y., Essawy, H., Zhao, C., Wu, Z., Zhou, X., Hou, D., & Du, G. (2022). Gelatinized starch-furanic hybrid as a biodegradable thermosetting resin for fabrication of foams for building materials. *Carbohydrate Polymers, 298*. https://doi.org/10.1016/j.carbpol.2022.120157

Zhang, L., Zhao, J., Zhang, Y., Li, F., Jiao, X., & Li, Q. (2021). The effects of cellulose nanocrystal and cellulose nanofiber on the properties of pumpkin starch-based composite films. *International Journal of Biological Macromolecules, 192*, 444–451. https://doi.org/10.1016/j.ijbiomac.2021.09.187

Zhang, Q., Wang, Z., Zhang, C., Aluko, R. E., Yuan, J., Ju, X., & He, R. (2020). Structural and functional characterization of rice starch-based superabsorbent polymer materials. *International Journal of Biological Macromolecules, 153*, 1291–1298. https://doi.org/10.1016/j.ijbiomac.2019.10.264

Zhang, Z. X., Zhang, J., Lu, B. X., Xin, Z. X., Kang, C. K., & Kim, J. K. (2012). Effect of flame retardants on mechanical properties, flammability and foamability of PP/wood-fiber composites. *Composites Part B: Engineering, 43*(2), 150–158. https://doi.org/10.1016/j.compositesb.2011.06.020

Zhou, Y. G., & Zhang, Y. L. (2023). Hybrid reinforced effect of long carbon fiber and short glass fiber on polycarbonate foams. *Polymer Composites*. https://doi.org/10.1002/pc.27578

Zimmermann, M. V. G., da Silva, M. P., Zattera, A. J., & Campomanes Santana, R. M. (2017). Effect of nanocellulose fibers and acetylated nanocellulose fibers on properties of poly(ethylene-co-vinyl acetate) foams. *Journal of Applied Polymer Science, 134*(17). https://doi.org/10.1002/app.44760

Zimniewska, M., Rozańska, W., Gryszczynska, A., Romanowska, B., & Kicinska-Jakubowska, A. (2018). Antioxidant potential of hemp and flax fibers depending on their chemical composition. *Molecules, 23*(8). https://doi.org/10.3390/molecules23081993

Zuo, Y., Gu, J., Tan, H., Qiao, Z., Xie, Y., & Zhang, Y. (2014). The characterization of granule structural changes in acid-thinning starches by new methods and its effect on other properties. *Journal of Adhesion Science and Technology, 28*(5), 479–489. https://doi.org/10.1080/01694243.2013.843283